

THE VERY SOFT X-RAY SPECTRUM OF THE DOUBLE PULSAR SYSTEM J0737–3039

A. POSSENTI¹, N. REA², M. A. McLAUGHLIN^{3,4}, F. CAMILO⁵, M. KRAMER⁶, M. BURGAY¹, B. C. JOSHI⁷, A. G. LYNE⁶*Draft version September 9, 2021*

ABSTRACT

We present the results of an 80 ks *Chandra* ACIS-S observation of the double pulsar system J0737–3039. Furthermore, we report on spectral, spatial and timing analysis of the combined X-ray observations performed so far for this system. Fitting a total of ~ 1100 photons, we show that the X-ray spectrum of the J0737–3039 system is very soft, and not satisfactorily modeled by a simple blackbody or an atmospheric model. However, it is not possible yet to discriminate between a predominantly non-thermal and a predominantly thermal origin for the X-ray emission.

Adopting a simple power-law emission model, the photon index ($\Gamma = 3.7 \pm 0.4$, 90% confidence interval) and the implied conversion efficiency of the rotational energy of PSR J0737–3039A into X-ray emission ($4.1 \pm 0.5 \times 10^{-4}$, for a distance to the source of 500 pc) are compatible with the X-ray photons being emitted in the magnetosphere of PSR J0737–3039A. This hypothesis is also supported by the absence of detectable X-ray orbital modulation (up to $\sim 20\%$, 3σ) or any X-ray nebular emission and it is in agreement with the high ($\gtrsim 75\%$) X-ray pulsed fraction of PSR J0737–3039A.

A two blackbody or a Comptonized blackbody model also reproduce the data, and the upper limit to the value of the hydrogen column density, $N_H \lesssim 1 \times 10^{20} \text{ cm}^{-2}$, is in better agreement (with respect to the power-law model) with the Galactic N_H in that direction and at that distance. For the two blackbody model the implied emission radii and temperatures are also compatible with those seen in other recycled pulsars, calling for the bulk of the X-ray photons being originated from heated regions at the surface of pulsar A. On the other hand, in the Comptonized blackbody model, the electron temperature seems to be significantly smaller than in other similar objects.

Subject headings: pulsars: individual (PSR J0737–3039A, PSR J0737–3039B, PSR B1534+12) — stars: neutron: pulsar — X-ray: stars

1. INTRODUCTION

The J0737–3039 system is a unique celestial object. It comprises a 23 ms pulsar (PSR J0737–3039A, hereafter pulsar A; Burgay et al. 2003) and a 2.8 s pulsar (PSR J0737–3039B, hereafter pulsar B; Lyne et al. 2004) revolving every 2.4 hr about their common center of mass along a somewhat eccentric ($e \sim 0.088$) and highly inclined ($\sim 89^\circ$; Kramer et al. 2006) orbit.

Timing observations in the radio band have allowed the most precise test of general relativity in strong field to date and promise to supersede the best Solar-system tests of gravitational theories (Kramer et al. 2006). Various unprecedented phenomena have also been detected at radio wavelengths, opening the possibility of studying the so far inaccessible pulsar magnetosphere: e.g. orbital modulation of the flux density from pulsar B (Lyne et al. 2004), modulation of the lightcurve of A during the eclipse at the (full and half) spin period of pulsar B (McLaughlin et al. 2004a), and the emission of pulsar B being affected by radiation of pulsar A (McLaughlin et al. 2004b).

The J0737–3039 system is also one of only two double neutron star (DNS) binaries that have been detected in the X-ray band. This is particularly interesting, since many

different X-ray emission processes may simultaneously be at work in this system, producing different spectral signatures. (1) X-rays could have the quasi-thermal spectrum expected if the surface(s) of pulsar A and/or pulsar B are heated by a flow of particles accelerated in the pulsar magnetosphere, depositing their kinetic energy on the magnetic polar cap(s). Cheng & Ruderman (1980) and Arons (1981) predicted an almost uniform temperature for such hot spots, whereas Zavlin & Pavlov (1998) suggested that the heated region is larger than the nominal pulsar polar cap and can be approximated with a central area at higher temperature surrounded by a larger rim at a lower temperature. Alternatively, (2) X-rays could show the power-law non-thermal spectrum associated with magnetospheric emission. Applying the outer gap model (see e.g. Cheng & Zhang 1999), the X-rays are mostly produced by synchrotron emission in an outer gap, whereas in a polar cap model (e.g. Zhang & Harding 2000) X-ray are generated by resonant inverse Compton scattering off thermal X-ray photons. In both cases the expected photon index Γ of the power-law spectrum is $\lesssim 2$, although observations indicate a somewhat larger range $\Gamma \sim 1 - 3$ (Zavlin 2006; Li et al. 2007). A further possibility (proposed by Bogdanov et al.

¹ INAF – Osservatorio Astronomico di Cagliari, Loc. Poggio dei Pini, 09012 Capoterra (CA), Italy; possenti@ca.astro.it

² University of Amsterdam, Astronomical Institute “Anton Pannekoek”, 1098 SJ, Amsterdam, The Netherlands

³ Department of Physics, West Virginia University, Morgantown, WV 26506, USA

⁴ National Radio Astronomy Observatory, Green Bank, WV, 24944, USA

⁵ Columbia Astrophysics Laboratory, Columbia University, New York, NY 10027, USA

⁶ University of Manchester, Jodrell Bank Observatory, Macclesfield, Cheshire, SK11 9DL, UK

⁷ National Centre for Radio Astrophysics, Ganeshkhind, Pune 411007, India

2006 e.g. for the case of PSR J0437–4715) is that (3) the X-ray emission comprises a thermal component resulting from polar cap(s) heating and a power-law component due to inverse Compton scattering of the soft thermal photons by energetic particles. Processes occurring at the termination shock may also be observed as in pulsar wind nebulae (PWN; see Gaensler & Slane 2006). In particular Lyutikov (2004) and Granot & Mészáros (2004) showed that a (4a) non-thermal X-ray spectrum may originate in the “collision” between pulsar A’s wind and pulsar B’s magnetosphere. This hypothesis is supported by the unusual aforementioned phenomena observed in the radio band, implying a strong interaction between the energetic flux of electromagnetic waves and particles released by pulsar A and the magnetosphere of pulsar B. Granot & Mészáros (2004) also noticed that (4b) non-thermal X-ray photons with the typical spectral index of a PWN (1.5–2.1, see e.g. Li et al. 2007) may be released by the pulsar A’s wind just behind the shock caused by the systemic motion of the binary in the interstellar medium.

We note that pulsar A is a mildly recycled pulsar with an intermediate value of inferred surface dipole magnetic field ($B_A \sim 6 \times 10^9$ G). The only other similar source detected in the X-ray band (Kargaltsev et al. 2006) is PSR B1534+12A having $B \sim 1 \times 10^{10}$ G, and whose distance (~ 1 kpc; Stairs et al. 2002) is about twice as large as that of pulsar A ($d \sim 500$ pc), as inferred from the pulsar dispersion measure and a model for the Galactic electron density (Cordes & Lazio 2002; note that a preliminary determination of d from timing parallax is also consistent with this value, Kramer et al. 2006). Therefore pulsar A is a promising object for investigating the nature of the X-ray emission in a transition source between the fully recycled millisecond pulsars (MSPs) with B in the $10^8 - 10^9$ G range (see e.g. Zavlin 2006 for a review) and the middle-aged or young pulsars having $B \gtrsim 10^{12}$ G (see e.g. Li et al. 2007 for a listing of those detected in X-rays).

The results of three *Chandra* and one *XMM-Newton* pointings of the J0737–3039 system have already been published. The first short *Chandra* pointing (see Table 1) allowed detection of ~ 80 photons from the binary (McLaughlin et al. 2004c), whereas the second longer *XMM-Newton* exposure resulted in ~ 400 useful MOS1+MOS2 photons (Pellizzoni et al. 2004). Even the combination of these two data sets (Campana et al. 2004; Kargaltsev et al. 2006) did not provide strong constraints on the spectrum of the source. Campana et al. found that the data were compatible with both a single blackbody (BB) with effective temperature 0.20 ± 0.02 keV (90% confidence level) and emission radius 75_{-9}^{+30} m, or with a single power-law (PL) having photon index $\Gamma = 4.2_{-1.2}^{+2.1}$. They also found that the combination of a BB plus a PL with $\Gamma = 2$ appeared statistically acceptable, although the additional PL component was not required by the data.

The *XMM-Newton* pointing allowed the first useful timing analysis, showing that no variation in the X-ray flux was visible along the orbit, up to a maximum degree of modulation of $\sim 40\%$ (99% confidence level) assuming a

sinusoidal shape for the light-curve (Pellizzoni et al. 2004). The second and third *Chandra* observations used the high temporal resolution of the HRC-S detector, resulting in the discovery that the bulk of the X-ray emission from the J0737–3039 system is pulsed at the rotational period of pulsar A (Chatterjee et al. 2007). The X-ray profile is double-peaked with rapidly rising narrow peaks and a high pulsed fraction of $74_{-14}^{+18}\%$. Folding the photons in orbital phase, Chatterjee et al. (2007) likewise did not find any evidence for X-ray flux variability along the orbit, nor any modulation of the X–emission at the spin rate of pulsar B⁸.

In this paper we present (§2.1) a new 80 ks *Chandra* ACIS-S observation of the J0737–3039 system, performed on 2006 June, which resulted in ~ 500 additional photons. We then report on spectral, spatial (§3) and timing (§4) analysis carried out by combining this new dataset with all previous suitable X-ray observations of this source (§2.2). The results are discussed in §5.

2. OBSERVATIONS AND DATA REDUCTION

2.1. New *Chandra* data

The J0737–3039 system was observed on 2006 June 6–7 (ObsID 5501), for 80 ks with the *Chandra* Advanced CCD Imaging Spectrometer (ACIS). The ACIS CCDs S1, S2, S3, S4, I2 and I3 were on during the observation. The back-illuminated ACIS-S3 CCD was positioned on the nominal target position and the source was observed in Timed Exposure (TE) and in VFAINT mode with a time resolution of 3.241 s. Standard processing of the data was performed by the *Chandra* X-ray Center to Level 1 and Level 2 (processing software DS 7.6.7.2), while we used CIAO (version 3.4) to complete the data reduction. All the standard data cleaning and astrometry correction procedures⁹ have been applied to the data. The source was clearly detected at sky coordinates (J2000.0) R.A. = $07^{\text{h}}37^{\text{m}}51.24^{\text{s}}$ and Decl. = $-30^{\circ}39'40.66''$. We performed a boresight correction matching 4 X-ray sources lying close to the J0737–3039 system with the 2MASS catalogue, deriving a final positional error on these coordinates of $0.4''$ at 99% confidence level. This position is compatible with the more accurate positions derived from radio timing (Kramer et al. 2006) and interferometry (Chatterjee, Goss & Brisken 2005), and with that determined from a previous *Chandra* observation (McLaughlin et al. 2004c).

For the timing analysis, we extracted the source events from a circular region of $2''$ radius centered on the source coordinates (this ensures enclosure of more than 90% of the source photons), and we used a $5''$ extraction radius for the spectral analysis. Background events have been acquired from regions of similar areas, and located on the same S3 CCD, but chosen as far as possible from the source. The choice of two different extraction radii was driven by the plan to use the H statistic in the orbital modulation search (see §4), and therefore requiring a negligible number of background counts in the source event file. For the spectral analysis this is not an issue, and we have chosen a wider extraction radius to collect more counts in order to

⁸ During the refereeing process of this paper, the results of an additional *XMM-Newton* pointing have been presented by Pellizzoni et al. (2008): the timing capability of the pn detector and the long duration of the integration allowed them to detect pulsed X–ray emission also from pulsar B in part of the orbit

⁹ http://cxc.harvard.edu/ciao/guides/acis_data.html

better constrain the background spectrum, and safely subtract it from the source (see §2.3 and §3). For both timing and spectral analyses we used all photons in the 0.3–8 keV energy range. The resulting source background-subtracted count rate is $6.3 \pm 0.3 \times 10^{-3}$ counts s^{-1} .

2.2. Previous *Chandra* and *XMM-Newton* datasets

Spectral, spatial and timing analyses (see §2.3) have been performed joining the observation presented in §2.1 with all the suitable datasets available to date (see Table 1).

The *XMM-Newton* observation of 2004 April was processed using SAS version 7.1.0, cleaned for solar and proton flares (see Table 1 for the resulting exposure times), and employing the most up-to-date calibration files (CCF release in 2006 November). The PN camera was observing in Timing mode, the MOS1 in Prime Full Window mode, and the MOS2 in Small Window mode (0.03 ms, 2.6 s and 0.3 s timing resolution for PN, MOS1 and MOS2, respectively). For all of our analyses we used only MOS1 and MOS2 data, since the PN observation was highly background dominated (because of the Timing mode set-up). We applied an extraction radius for events and spectra of $15''$ for MOS1 and MOS2 data (this ensures enclosure of more than 90% of the source photons). We used for timing and spectral analyses only photons in the 0.3–2.2 keV energy range because above 2.2 keV the source was highly background dominated.

The *Chandra* ACIS-S observation taken in 2004 January was re-analyzed using the same procedures and extraction regions as for the new dataset presented in §2.1.

The two *Chandra* HRC-S observations performed in 2006 were reprocessed using standard procedures for HRC analysis¹⁰. We first checked the data for the presence of solar flares and extracted a new observation-specific bad-pixel file. We then ran a degap correction, and corrected the astrometry for any processing offset, starting from Level 1 files. Source and background events have been extracted from two circular regions of $1.2''$ radius each: one centered at the source position (this ensures enclosure of more than 90% of the source photons), and the other as far as possible from the source.

For all these archival observations we found results which are consistent with those already published for each dataset (McLaughlin et al. 2004c; Pellizzoni et al. 2004; Campana et al. 2004; Kargaltsev et al. 2006; Chatterjee et al. 2007). Furthermore, within the limited photon statistics available, the results from all observations were consistent with each other. Therefore, when it was relevant/useful, we added some of the observations together, in order to improve the statistics.

2.3. Analysis

For the spectral analysis we made use only of the *Chandra* observation reported in §2.1 and of the *XMM-Newton* observation of 2004 April (see Table 1). The *Chandra*

HRC-S camera does not have spectral capabilities, and we have chosen not to include the first *Chandra* ACIS-S observation because the low number of counts would have prevented us from using the χ^2 statistic as a measure of the goodness of our spectral modeling. That left us with a total of 1095 ± 15 photons (corrected for background) for our spectral analysis. The spectra have been re-binned (before the background subtraction) to have at least 15 (for *Chandra*) and 25 (for *XMM-Newton*) counts per spectral bin; hence we ended with a total of 31 spectral bins for ACIS-S in the 0.3–8 keV energy range, and 10 and 9 spectral bins for MOS1 and MOS2, respectively, in the 0.3–2.2 keV energy range. The different counts per bin used for *Chandra* and *XMM-Newton* data reflects the need of having a similar signal-to-noise (S/N) per bin for both observations, hence compensating for the higher background of the *XMM-Newton* observation.

Response matrices were built for each spectrum in the standard manner¹¹. Finally, several emission models were fitted to the data using XSPEC versions 11.3 and 12.1 and adopting an interstellar absorption component modeled by `phabs` using solar abundances from Lodders (2003). We added a systematic error of 5% in order to account for inter-calibration between the different instruments¹². As a further inter-calibration check, we applied all resulting models (excluding the 5% systematics) to the *Chandra* data alone, and found consistent results.

For spatial analysis we only used HRC-S and ACIS-S datasets, because of the poorer *XMM-Newton* spatial resolution with respect to *Chandra*. We built the instrumental Point Spread Function (PSF) for each of the *Chandra* observations making use of the *ChaRT* and the *MARX* software packages¹³. For all the PSFs, we used the source spectrum (see §3) as an input for the energy distribution of the PSF itself. We then created an image for our ACIS-S and HRC-S PSFs, and fitted it to the data, searching for any disagreement between either the one or the two dimensional source profiles and the instrumental PSFs.

For timing analysis we used all the datasets listed in Table 1. This gives us an intrinsic time resolution in orbital phase of about $1/2700$ (set by ACIS-S, which has the worst time resolution of the 5 datasets, see caption of Table 1). Only the portions of any observation covering an integer number of orbits were considered, thus ensuring uniform coverage of orbital phase for each instrument; the last operation left us with 1442 photons (~ 125 of which we estimate are due to the background) out of a total of 1573 (~ 170 due to the background), spread over 25 orbits (see Table 1). The times of arrival (TOAs) of the photons were first referenced to the barycenter of the Solar System, assuming the accurate radio position from Kramer et al. (2006) and adopting the JPL planetary ephemeris DE405. Then, we used TEMPO¹⁴ and the timing solution tabulated in Kramer et al. (2006) to calculate the orbital phases (with respect both to the ascending node of PSR J0737–3039A and to its periastron) associated both with

¹⁰ http://cxc.harvard.edu/ciao/guides/hrc_data.html

¹¹ For ACIS-S see <http://cxc.harvard.edu/ciao/threads/all.html>; for MOS see <http://xmm.vilspa.esa.es/sas/7.1.0/documentation/threads/>.

¹² For more details see http://xmm.esac.esa.int/external/xmm_sw_cal/calib/cross_cal/index.php.

¹³ <http://cxc.harvard.edu/chart/threads/marx/>

¹⁴ <http://www.atnf.csiro.au/research/pulsar/timing/tempo>

the list of 1442 barycentric on-source TOAs and with the list of barycentric TOAs collected from the background area. Background-subtracted light-curves as a function of orbital phase were then produced and inspected for the presence of modulation.

3. SPECTRAL AND SPATIAL RESULTS

We first tried to model the spectrum using single components (see Table 2). Models consisting of an absorbed blackbody (BB, XSPEC model `bbbody`; see Fig. 1) or an absorbed atmospheric emission (NSA, XSPEC model `nsa`) are not compatible with the data. The first has $\chi_\nu^2 = 2.3$ (see Table 2; χ_ν^2 is the reduced χ^2) and a null hypothesis probability (n.h.p.) of 4×10^{-6} . The second has $\chi_\nu^2 = 1.8$, and a n.h.p. of 2×10^{-3} .

On the other hand, both an absorbed power-law (PL, XSPEC model `powerlaw`: $\chi_\nu^2 = 1.25$, n.h.p. of 9×10^{-2}) and an absorbed thermal bremsstrahlung model (BSS, XSPEC model `BREMSS`: $\chi_\nu^2 = 1.28$, n.h.p. of 8×10^{-2}) can satisfactorily reproduce our data. The PL model (see Fig. 1) has a large photon index $\Gamma = 3.7 \pm 0.4$ (here and everywhere in the paper, we use 90% confidence intervals, i.e. $\Delta\chi^2 = 2.71$) and an equivalent hydrogen column density $N_H = (1.6 \pm 0.6) \times 10^{21} \text{ cm}^{-2}$. Figure 2 shows a contour plot of these parameters. For a distance to the J0737–3039 system of 500 pc, the unabsorbed flux (see Table 2) translates into a luminosity of $(2.4 \pm 0.3) \times 10^{30} \text{ ergs s}^{-1}$ in the 0.3–8 keV range.

The BSS model requires a much lower N_H with respect to the PL model, with an equivalent temperature of $kT = 0.6 \pm 0.1 \text{ keV}$ and a 0.3–8 keV luminosity of $(0.9 \pm 0.3) \times 10^{30} \text{ ergs s}^{-1}$. However, it is possible to show that¹⁵ these best fit parameters for the emitting nebula would imply a dispersion measure for the system, $\gtrsim 10^{22} \text{ cm}^{-2}$, two orders of magnitude larger than the observed value $\text{DM}_{\text{obs}} = 1.5 \times 10^{20} \text{ cm}^{-2}$.

Given their possible physical relevance, we have also explored the blackbody plus power-law (BB+PL), the neutron star atmosphere plus power-law (NSA+PL), the double blackbody (BB+BB) and the Comptonized blackbody (compBB) models. The combination of a BB (or a NSA) with a PL does not significantly vary the single PL parameters or improve the fit, despite the additional free parameters ($\chi_\nu^2 \sim 1.28$, n.h.p. of 7×10^{-2}). In particular, for all the statistically acceptable fits, the additional thermal component accounts only for $\lesssim 2\%$ of the total 0.3–8 keV unabsorbed luminosity. In Table 2, we report on the BB+PL model showing the maximum contribution from the blackbody (it has the same BB temperature, $kT = 0.18 \text{ keV}$, of the best-fit blackbody when fitted alone). At a distance of 500 pc, the corresponding BB emission radius is $R_{bb} = 18 \pm 12 \text{ m}$, significantly smaller than the nominal polar cap radius of both pulsar A ($\sim 1 \text{ km}$) and pulsar B ($\sim 90 \text{ m}$). Also note that a BB+PL model with $\Gamma = 2$ (still acceptable using only the data taken in 2004; Campana et al. 2004) is now ruled out ($\chi_\nu^2 \sim 1.81$, n.h.p. of

7×10^{-4}). On the contrary, a BB+BB model is compatible with the data (see Fig. 1), although it does not statistically improve the quality of the fit (see Table 2): the coolest BB ($kT_1 = 0.10 \pm 0.01 \text{ keV}$) contributes $\sim 60\%$ to the total luminosity with an emission radius $R_{bb,1} = 360 \pm 150 \text{ m}$, while the warmest BB ($kT_2 = 0.30 \pm 0.05 \text{ keV}$) has a tiny $R_{bb,2} = 20 \pm 10 \text{ m}$. We note that it has a much lower N_H with respect to the PL model. Following the fitting prescription by Bogdanov et al. (2006) for PSR J0437–4715 (i.e., fixing the value of N_H and assuming a thermal bath of scattering pairs e^\pm at a temperature $\sim kT_e = 150 \text{ keV}$), a Comptonized blackbody model (compBB, XSPEC model `compbb`) is completely ruled out ($\chi_\nu^2 = 1.95$, n.h.p. of 8×10^{-5}). Allowing kT_e to vary, the χ_ν^2 improves significantly (see the best fit parameters in Table 2), although the fit is still statistically worse than that of the PL or BB+BB models. The relatively small number of available photons prevent performing a meaningful fit for even more complicated multi-component models, such as a two blackbody plus a powerlaw (BB+BB+PL) model or a two temperature Comptonized model (compBB+compBB).

We note that the χ_ν^2 resulting from our best fits (those for the PL model and the BB+BB model) are acceptable, but not very close to the optimal $\chi_\nu^2 = 1$ (see Table 1). As explained in §2.2 and §2.3, we have also fitted the spectra from *Chandra* and *XMM-Newton* data separately, obtaining compatible parameters and χ_ν^2 values in the same range as above. Therefore inter-calibration should not have a major role in determining the values of χ_ν^2 . We have then also searched for spectral and flux variability using the whole X-ray datasets, and also dividing them in time-slices (see also §4), but no such variability has been detected (however, the limited number of counts in each time-resolved spectrum makes this non detection not very constraining). Increasing the number of components in the adopted model also does not help a lot, as demonstrated e.g. comparing the χ_ν^2 of the best fit PL and BB+PL models. Of course, it cannot be excluded that even more complicated spectral models will finally improve the values of χ_ν^2 . However the effect of the interstellar abundances might also be a promising explanation: e.g. excluding 3 bins in the spectral fit (one centered at 0.95 keV and two bracketing the range 0.60–0.75 keV) allows us to reach $\chi_\nu^2 = 1.02$ even for the very simple PL model (leaving basically unchanged the best fit parameters). This improvement may be due to the presence of a few edges in the photoelectric absorption that are not properly modeled when adopting solar abundances. We tried to leave the abundances of the single elements free in `vphabs`, but the low available counts (compared with the increased number of fitted parameters) does not make this modeling statistically significant. So, we think that a much better photon statistics are needed for assessing if the not optimal value of the best fit χ_ν^2 is due to a poor spectral modeling either of the source or of the matter along the line-of-sight, or something else.

¹⁵ Given the best fit values of kT and luminosity, we can follow Grindlay et al. (2002) to estimate $\epsilon \sim \bar{n}^2 R^3 \sim 7 \times 10^{52} \text{ cm}^{-3}$ (where R is the typical size of the BSS emitting nebula and \bar{n} is the mean plasma density in that volume, assuming homogeneity and total charge neutrality). Since a large fraction of the X-ray emission from the system is pulsed (Chatterjee et al. 2007) at the spin period of A, $P_A \sim 22.7 \text{ ms}$, the size of the emitting region should be $R \lesssim cP_A$. Combining these two constraints, we can estimate the contribution DM_{neb} of the X-ray BSS emitting nebula to the dispersion measure; it turns out $\text{DM}_{\text{neb}} \sim \bar{n}R \sim \epsilon^{1/2} R^{-1/2} \gtrsim 10^{22} \text{ cm}^{-2}$. Even assuming a negligible contribution due to the plasma in the intervening interstellar medium (ISM) along the line-of-sight, the total dispersion measure $\text{DM}_{\text{ISM}} + \text{DM}_{\text{neb}}$ can hardly be reconciled with the observed value DM_{obs} for the system.

Finally, applying the procedure for the spatial analysis described in §2.3, we did not detect any diffuse emission neither in the *Chandra*HRC datasets (as also reported by Chatterjee et al. (2007) using a different analysis method), nor in our new ACIS data. In Figure 3 we report on the comparison between the new ACIS data of the J0737–3039 system with the one dimensional *Chandra* PSF, built as described in §2.3, as a function of the angular distance from the source position. Assuming a power-law spectra spanning the range $\Gamma = 2-4$, this translates to a conservative (averaged over an annulus of $0.5''-2''$) upper limit on the X-ray luminosity of a diffuse component of $\sim 2 \times 10^{30}$ ergs s^{-1} (90% confidence level, 0.3–8 keV band).

4. LIMITS ON ORBITAL MODULATION

Figure 4 shows the background-subtracted light-curves of the J0737–3039 system obtained by folding all the available X-ray photons according to the procedure described in §2.3, and binning into 20 orbital phase bins. Since the periastron of the system advanced by about 0.11 in orbital phase during the time elapsed between the first and the last observation, we produced histograms which are phased both with respect to the periastron of the orbit and with respect to the ascending node of the orbit of pulsar A. The first choice (hereafter light-curve LC_{per}) aims to reveal possible modulations in the X-ray curve related to the changing relative position and orientation of the two neutron stars along the orbit (e.g. the variation of their distance). The second option (hereafter light-curve LC_{asc}) may better reveal evidence for modulations related to the orientation of the system with respect to the line-of-sight.

No statistically significant variations in the X-ray flux were detected in either of the two folded light-curves. In particular, applying Pearson χ^2 statistics gives $\chi^2_{\nu} = 1.28$ and $\chi^2_{\nu} = 1.07$ (with $\nu = 19$ degrees of freedom) for LC_{per} and LC_{asc} , respectively, corresponding to probability of $\sim 17\%$ and $\sim 37\%$ that the histograms are drawn from a uniform distribution. Since the results of Pearson statistics depend on the adopted center of the bins, the values of χ^2_{ν} reported above are the average over 100 different choices of bin center for light-curves with 20 bins. We have folded the data with various combinations of number of bins (from 4 to 32) and number of trial bin center (in agreement with the typical number of photons in each bin); all the resulting light-curves are compatible (at 3σ) with a constant photon flux along the orbit.

In order to overcome the dependency of the results on the binning, we also adopted the H statistic, which appears to be the best test for a wide range of physically plausible light-curves (De Jager et al. 1989). The value of H is calculated as $H = \text{Max}(Z_m^2 - 4m + 4)$, where Z_m^2 is the family of Rayleigh statistics and the smoothing parameter m spans the interval 1 – 20. Unfortunately, this test cannot be safely applied to the *XMM-Newton* data, since the unbinned data are contaminated (at $\sim 25\%$ level) by the background photons. Limiting the analysis to the 1010 *Chandra* photons (of which only $\lesssim 2\%$ may be due to the background) results in $H = 2.24$ at $m = 1$ when the orbital phases are referred to the periastron and $H = 2.38$ at $m = 1$ when referred to ascending node. Hence, the chance probabilities that we are sampling a uniform distribution are $\sim 41\%$ and $\sim 39\%$, respectively.

Finally, we have tried to estimate an upper limit to the pulsed fraction (i.e. the degree of modulation) $p_f = (\text{Max} - \text{Min})/(\text{Max} + \text{Min})$ of the orbital light-curves. In order to do that, we have used a Monte Carlo code for simulating sinusoidally modulated light-curves, having on average the same count-rate per bin of the observed light-curves. For any given value of p_f , about 1000 of these light-curves (with randomly chosen phase) were generated and then subjected to the Pearson statistic in order to estimate the probability of their being drawn from a uniform distribution. This yielded, assuming a sinusoidal modulation of arbitrary phase, $p_f < 18\%$ at 3σ , a limit more than 2 times smaller than that of Pellizzoni et al. (2004).

It has been shown (Chatterjee et al. 2007) that a large fraction of the X-ray emission from the system is pulsed at the spin period of pulsar A. Therefore, our conclusions above mostly constrain orbital variations of the pulsed emission from pulsar A. Only HRC-S data have enough time resolution for selecting photons in the off-pulse phase of the rotation of pulsar A ($\sim 20\%$ of the pulsar A's spin period); the analysis of the orbital variations for this small subset of photons (~ 30) was first performed by Chatterjee et al. (2007). Repeating their analysis, we likewise did not find any significant modulation. Given the poor photon statistics, our derived upper limit to the pulsed fraction of $p_f \lesssim 90\%$ (at 3σ for a sinusoidal modulation) is not very constraining.

5. DISCUSSION

The ~ 500 additional photons made available by the new *Chandra* observation allowed us to significantly reduce the uncertainties on the spectral parameters of the J0737–3039 system and to confirm that it has a very soft X-ray spectrum. In particular, in contrast to previous attempts based on a much smaller number of photons (McLaughlin et al. 2004c; Pellizzoni et al. 2004; Campana et al. 2004), our analysis shows that a simple absorbed blackbody model does not acceptably describe the X-ray spectrum of the J0737–3039 system (see Fig. 1). The same holds true for a simple thermal emission model (assuming a uniform temperature of emission) corrected for the radiative transport in the atmosphere of the neutron star. Although it is compatible with the data, a thermal bremsstrahlung spectrum is also excluded on the basis of a comparison with the observed value of the dispersion measure (see §3).

However, the ~ 1100 available photons do not allow us yet to discriminate between a predominantly thermal and a predominantly non-thermal emission. In the following, we discuss these two options and their ramifications.

5.1. Thermal emission: heated polar caps

Thermal emission released from relatively small areas having unequal temperatures is not unexpected in recycled pulsars (Bogdanov et al. 2006; Zavlin 2006). As reviewed in §1, it could be ascribed to the effects of the bombardment of the neutron star surface by particles accelerated in the magnetosphere of pulsar A, which is the most energetic of the two pulsars (cooling of the neutron star interior cannot yield significant X-ray emission for pulsars older than ~ 50 Myr, as appears to be the case for the J0737–3039 system; Lorimer et al. 2007). The temperatures of the BB+BB model for the J0737–3039 system

(see Table 1) are somewhat higher and the emission radii are smaller than those inferred (Zavlin 2006) for the MSPs J0437–4715 ($kT_1 \sim 0.04$ keV, $kT_2 \sim 0.12$ keV, $R_{\text{bb},1} = 2.6$ km, $R_{\text{bb},2} = 0.4$ km) and J0030+0451 ($kT_1 \sim 0.07$ keV, $kT_2 \sim 0.18$ keV, $R_{\text{bb},1} = 1.4$ km, $R_{\text{bb},2} = 0.1$ km) by applying a model in which the magnetic poles are surrounded by a weakly magnetized hydrogen atmosphere (Zavlin et al. 1996). The discrepancy could possibly be corrected by likewise including the effects of the atmosphere in the J0737–3039 system spectral model. (In fact, a neutron star H-atmosphere spectrum tends to decrease the best-fit temperature and to increase the emission radius with respect to a simple blackbody).

The presence of hot spot(s) may be also responsible for the observed double peaked X-ray light-curve, modulated at the spin period of pulsar A (Chatterjee et al. 2007). A difficulty with this interpretation is due to the very high observed pulsed fraction $p_f = 74^{+18}_{-14}\%$ (1σ error; Chatterjee et al. 2007) of the X-ray light-curve. In fact, the strong gravitational bending which is experienced by radiation emitted at the surface of a non magnetized neutron star limits the pulsed fraction produced by an isotropically emitting hot spot to $\lesssim 30\%$ (Psaltis et al. 2000). Only the presence of strong surface magnetic fields $B_s \gg 10^{10}$ G can significantly increase the pulsed fraction (Page & Sarmiento 1996; Geppert et al. 2006), perhaps helping to account for sources like PSR J1119–6127 (a young, high- B pulsar), showing a thermal spectrum and $p_f \sim 75\%$ (Gonzalez et al 2005). However, the value of B_s for PSR J1119–6127 (4.1×10^{13} G) is well above that for pulsar A and all the other recycled pulsars. Thus, anisotropy in photon transport across a weakly magnetized neutron star atmosphere (e.g. Zavlin et al. 1996) has been invoked to increase the predicted pulsed fraction up to the values of 35–50% seen in the four recycled MSPs (including the aforementioned PSRs J0437–4715 and J0030+0451) whose X-ray emission is interpreted to be mostly thermal. It is still debatable if these atmospheric effects can really produce light-curves approaching as high values of p_f as those seen in pulsar A¹⁶. We also note that the X-ray pulse profiles of the thermally emitting MSPs display more sinusoidal and less spiky pulses than those shown by pulsar A.

5.2. Thermal emission: Comptonized spectrum

For PSR J0437–4715, Bogdanov et al. (2006) proposed that the predominantly thermal nature of the X-ray emission (due to heated polar caps) is complemented by the non-thermal emission due to weak Comptonization of the thermal (blackbody or hydrogen atmosphere) polar cap emission by energetic electrons/positrons of small optical depth, presumably in the pulsar magnetosphere and wind. In the case of the J0737–3039 system, this interpretation (see hypothesis (3) in §1) leads to a spectral modeling (see Table 2) having best fit parameters dissimilar with respect to those of PSR J0437–4715 ($kT_1 \sim 0.01$ keV,

$kT_2 \sim 0.25$ keV, $R_1 \sim 0.3$ km, $R_2 \sim 0.04$ km, and optical depth $\tau_1 \sim 0.09$ and $\tau_2 \sim 0.06$, respectively, Bogdanov et al. 2006). On a physical ground, this spectral modeling for the X-ray emission nicely fits with the hypothesis (see Harding & Muslimov 2002) that inverse Compton scattering (ICS) is the main responsible for pair production and particle bombardment of the polar caps in millisecond pulsars (Bogdanov et al. 2006). We note that future deep observations in the optical band of the J0737–3039 system may help discriminating this model with respect to a pure PL model of magnetospheric origin (see §5.3) and a BB+PL model (see §5.4): in fact no non-thermal contribution at optical wavelengths is expected from a Comptonized spectrum. On the other hand, it is not clear if the inclusion of the contribution of a tail of Comptonized photons to a predominantly thermal spectrum can alleviate the problem of the high pulsed fraction of the X-ray emission from pulsar A (see §5.1).

5.3. Non thermal emission: a magnetospheric origin

A non-thermal nature for the J0737–3039 system spectrum implies that the bulk of the X-ray emission ($\gtrsim 98\%$ in total luminosity) is described by a power-law with a steep spectral index $\Gamma > 3.3$ (at 90% confidence level). As to the origin of this emission, the most probable hypothesis calls for radiation released by charged particles accelerated in the magnetosphere of pulsar A. A simple scaling law $L_x \propto \dot{E}^\beta$ between X-ray luminosity and spin-down luminosity for recycled pulsars in the Galactic field ($\beta \sim 1.1$; Grindlay et al. 2002) predicts a 0.5–2.5 keV luminosity of $\sim 5 \times 10^{30}$ ergs s^{-1} for pulsar A. This is compatible with the observed 0.5–2.5 keV luminosity of $\sim 10^{30}$ ergs s^{-1} , considering the typical scatter (one order of magnitude) for the above correlation¹⁷. The constancy of the emission along the orbit (§4) supports this hypothesis, as does the shape of the X-ray pulse profile (Chatterjee et al. 2007), which shares common features (i.e. narrow peaks and rapid rise and decline from the maxima) with the light-curves of the 4 well-studied recycled MSPs having a predominantly non-thermal spectrum (J0218+4232, B1821–24, B1937+21, and B1957+20; see Zavlin 2006 for a gallery). Moreover, the p_f of the pulse profile nicely falls in the range of values (65 – 100%) observed for the four sources mentioned above.

A problem with the non-thermal emission hypotheses (it applies to §5.4 as well) is given by the derived value of $N_H \sim 1.5 \times 10^{21}$ cm^{-2} . While the value actually matches that expected for the the dispersion measure (assuming the typical average of 10 neutral H-atoms for each e^- along the line-of-sight), the J0737–3039 system is located inside the Gum Nebula, given its estimated distance of $d \sim 500$ pc. In this case, we do expect an enhanced DM value without a similar enhancement in N_H . In fact, other known pulsars at the same distance but located in different directions have an average DM that is ~ 5 times smaller¹⁸ than that of the J0737–3039 system. Furthermore, all analy-

¹⁶ Note that the pulsed fraction computed for the X-ray emission from pulsar A is calculated assuming that the whole X-ray luminosity comes from pulsar A. If other emission mechanisms contribute to the observed luminosity, the p_f of pulsar A may be significantly larger.

¹⁷ Applying the correlation of Possenti et al. (2002; having $\beta \sim 1.4$ in the 2–10 keV band), the predicted luminosity is about 20 times larger than that observed. The same holds true for the correlation obtained by Cheng et al. (2006) using a larger database. This large discrepancy may reflect the soft spectrum of pulsar A, whose luminosity is mostly confined below 2 keV, outside the band selected by Possenti et al. (2002) and Cheng et al. (2006)

¹⁸ <http://www.atnf.csiro.au/research/pulsar/psrcat/>

ses of the X-ray spectrum of the cooling neutron star RX J0720.4–3125 found N_H in the range $6 - 10 \times 10^{19} \text{ cm}^{-2}$. Since RX J0720.4–3125 and the J0737–3039 system are fortuitously close in position in the sky (the angular distance is ~ 4 degrees) and at similar distances (360 pc for RX J0720.4–3125, Kaplan, van Kerkwijk & Anderson 2007), it seems reasonable to expect that their foreground hydrogen columns should be similar. We also note that the N_H resulting from fitting the X-ray spectrum of the J0737–3039 system with the explored non-thermal models corresponds to $\sim 30\%$ of the full Galactic value obtained from the measurements of neutral hydrogen (Dickey & Lockman 1990). On the other hand, the assumed distance of J0737–3039 system is $\sim 5\%$ of the neutral path length through the disk along the line of sight to the system, as can be inferred from e.g. Fig. 3a of McClure-Griffiths et al. (2004). These considerations would indicate a value of N_H for the J0737–3039 system in the range $(0.2 - 0.3) \times 10^{21} \text{ cm}^{-2}$, closer to the best fit value obtained for the thermal models than for the non-thermal models. Taken at face value, this can be interpreted as a weakness for the non-thermal emission hypothesis. However, we also note that the value of N_H resulting from our fits with a PL (or a BB+PL) model is strongly dependent on the adopted abundances: using the older abundances from Anders & Grevesse (1989) we get a value of N_H which is about 1/3 of that resulting from the more recent abundances (Lodders 2003) used in this paper (with all the other best fit parameters almost unchanged).

The rotational energy loss $\dot{E}_A = 5.8 \times 10^{33} \text{ ergs s}^{-1}$ of pulsar A is similar to the values ($\dot{E} \sim 10^{33} - 10^{34} \text{ ergs s}^{-1}$) of the fully recycled thermally emitting MSPs (Zavlin 2006), whereas the fully recycled non-thermally emitting MSPs have much larger $\dot{E} \sim 10^{35} - 10^{36.5} \text{ ergs s}^{-1}$. As a consequence, if a non-thermal emission is predominant in the J0737–3039 system, the non-thermal luminosity cannot be simply dependent on the magnitude of the energy input from the pulsar. Although the surface magnetic fields B_s of the thermally emitting MSPs are comparable with those of the non-thermally emitting MSPs (with the notable exception of PSR B1821–24), the values of their magnetic field at the light cylinder $B_{lc} = B_s [2\pi R_{\text{ns}}/cP]^3$ (where R_{ns} is the neutron star radius and P the spin period) are different: $B_{lc} \sim 2 - 3 \times 10^4 \text{ G}$ for the thermal emitters, $B_{lc} \sim 2 - 9 \times 10^5 \text{ G}$ for the non-thermal ones. This may be an ingredient for explaining the different emission properties of the two classes of sources (Saito et al. 1997; Zavlin 2006), but the spectrum of pulsar A (in the hypothesis that it is non-thermal) does not fit this picture, since $B_{lc} \sim 5 \times 10^3 \text{ G}$, even lower than that of the MSPs with a thermal spectrum.

What certainly differentiates pulsar A both from the thermally and the non-thermally emitting MSPs (except PSR B1821–24, having $B_s \sim 2 \times 10^9 \text{ G}$) is the much larger value of the magnetic field close to the neutron star surface. This could play a significant role in a polar cap scenario. In particular, as already noted by Chatterjee et al. (2007), pulsar A is one of the very few recycled pulsars (see Fig. 1 of Harding, Usov & Muslimov 2005) located above the death line for curvature radiation of Harding & Muslimov (2002; PSR B1821–24 also satisfies this condition). De-

tailed calculations will be necessary to investigate if this property may help trigger significant non-thermal X-ray emission from pulsar A, despite the pulsar having a longer spin period and a smaller \dot{E} than the other non-thermal MSPs. The different values of P and B_s with respect to the known population of X-ray emitting MSPs may also be a factor for determining the unusually steep photon index of pulsar A. In fact, all of the catalogued fully recycled MSPs dominated by power-law emission show $\Gamma \lesssim 2$ (although values of $\Gamma \sim 2.5 - 3.0$ are not unheard in the population of non-recycled pulsars; see e.g. the recent compilation of Li et al. 2007).

Interestingly, the spectrum of the only other DNS detected in X-rays, the B1534+12 system, can also be fitted with a power-law¹⁹ having a very soft photon index $\Gamma = 3.2 \pm 0.5$ (Kargaltsev et al. 2006), comparable with that of the J0737–3039 system. Longer observations will be necessary to better constrain this soft supposedly non-thermal spectrum and to reveal if the X-ray flux is modulated at the spin period ($P = 37.9 \text{ ms}$) of PSR B1534+12. A positive result would confirm the indication emerging from our analysis, i.e. that a peculiarly soft X-ray emission originates from the mildly recycled pulsars.

5.4. Non-thermal emission: other processes

Two facts challenge the interpretation of the X-ray emission from the J0737–3039 system as due to a shock at the interface between pulsar A’s wind and pulsar B’s magnetosphere (see the hypothesis (4a) described in §1). On one hand, we observe an apparent lack of modulation of the X-ray flux with orbital phase (§4), while on the other hand, one detects a high degree of modulation at the spin-period of A (Chatterjee et al. 2007). In fact, relativistic beaming of the X-ray photons emitted at the shock front is expected to produce an orbital modulation of order $\lesssim 50\%$ (Arons & Tavani 1993, Granot & Mészáros 2004, Pellizzoni et al. 2004). Despite the improved statistics resulting from the combination of all the suitable photons collected so far, no orbital variation of the X-ray flux from the J0737–3039 system has been detected, with an upper limit to the orbital modulation of $\sim 20\%$ (for an assumed sinusoidal variation). A further prediction of the model (Granot & Mészáros 2004) is that variability of the shock emission at the spin rate of pulsar A would be significantly washed out due to the large ratio between the time of flight of the X-ray photons from pulsar A to pulsar B’s magnetosphere and the rotational period of pulsar A. This contrasts with the very high pulsed fraction of the light-curve folded at the period of pulsar A. As noticed by Chatterjee et al. (2007), the absence of this kind of shock emission may support a very high degree of magnetization of the pulsar wind close to pulsar A. In fact, for highly magnetized shocks, the higher the degree of magnetization, the smaller we expect the X-ray luminosity of the shock to be (Kennel & Coroniti 1984). On the other hand, since the energy budget is still favorable (up to about $3 \times 10^{31} \text{ ergs s}^{-1}$) may in principle be available for powering this shock emission; Lyutikov 2004), we cannot exclude that a component of the observed total luminosity comes from this process, producing an orbital modulation below our upper limit. In fact, a *Chandra* observation of PSR B1534+12 indicates

¹⁹ Given the poor photon statistics, at the moment the data for PSR B1534+12 cannot exclude a blackbody model (Kargaltsev et al. 2006)

a deficit of X-ray emission around apastron (Kargaltsev et al. 2006). Since the orbit of the B1534+12 system is more eccentric ($e = 0.274$) than that of the J0737–3039 system the shock emission may be much more modulated in the former binary²⁰, while the collision between pulsar A’s wind and pulsar B’s magnetosphere may still provide a fraction of the total luminosity with a low level of modulation. In particular, if the entire unpulsed emission ($\sim 25\%$ of the total luminosity of the J0737–3039 system; Chatterjee et al. 2007), should be ascribed to this process, the expected orbital modulation would be $\lesssim 12\%$.

Energetic considerations make questionable an interpretation of the X-ray photons as due to the emission of pulsar A’s wind behind the shock caused by the motion of the J0737–3039 system in the interstellar medium (hypothesis (4b) described in §1). In particular, the predicted X-ray flux for this process (Granot & Mészáros 2004) is $\sim 2 \times 10^{29}$ ergs s^{-1} (assuming a typical particle density of 10 cm^{-3} in the interstellar medium and the observed systemic velocity of the J0737–3039 system, $\sim 10 \text{ km s}^{-1}$; Kramer et al. 2006), i.e. an order of magnitude less than that observed (see Table 1). We note that the derived upper limits ($\sim 2 \times 10^{30}$ ergs s^{-1} , see §3) on the luminosity of any diffuse emission around the position of the J0737–3039 system are not yet very constraining for the presence of a PWN. In fact, adopting the recent scaling law of Li et al. (2007) (and allowing for the typical scatter of one order of magnitude in the correlation) the expected luminosity in the 0.3–8 keV band of a PWN (if any) powered by the rotational energy loss of pulsar A ($\dot{E}_A = 5.8 \times 10^{33}$ ergs s^{-1}) should be $\lesssim 4 \times 10^{29}$ ergs s^{-1} . Nevertheless, this luminosity estimate, the high pulsed fraction of the emission at the spin period of pulsar A and the very soft spectrum (strongly at variance with the photon indexes seen in PWNs, see §1) permit us to conclude that a putative PWN can give only a negligible contribution to the energy budget of the X-ray emission from the J0737–3039 system.

5.5. Summary

Our analysis unambiguously indicates that the X-ray emission of the J0737–3039 system is characterized by a very soft spectrum. However, on the basis of the available data, we cannot discriminate between a predominantly

thermal and a predominantly non-thermal origin for this spectrum.

In the thermal emission hypothesis, the X-ray photons of the J0737–3039 system may (i) originate from two roughly concentric regions on the surface of pulsar A, heated to different temperatures by particles accelerated in the magnetosphere of pulsar A and impinging onto the neutron star, or may (ii) result from the combination of heated polar cap(s) emission and non-thermal photons scattered in inverse Compton processes in the pulsar magnetosphere. The high pulsed fraction (at the spin period of pulsar A) of the X-ray emission is a problem for these interpretations.

In the predominantly non-thermal emission hypothesis, magnetospheric emission from pulsar A may provide the bulk of the X-ray flux and easily explain the high pulsed fraction of the emission. A smaller contribution to the X-ray luminosity - due to either the interaction between pulsar A’s wind and pulsar B’s magnetosphere or to a thermal emission from heated caps - cannot be excluded, but it is not required by the available observations. The relatively high value of N_H (when compared with the assumed distance of the source) is the main difficulty with this interpretation.

The very soft nature of the spectrum appears to be echoed in the spectrum of the only other mildly recycled pulsar detected so far in the X-ray band, PSR B1534+12. This may corroborate the hypothesis that mildly recycled pulsars constitute a new class of neutron star X-ray emitters, undergoing different emission processes with respect to those modeled for the fully recycled pulsars. If this holds true, their study will be particularly important for understanding how different values of spin period and surface magnetic field may affect the mechanisms of X-ray production in rotation-powered neutron stars.

The authors thank the anonymous referee for a careful reading of the manuscript, and the very helpful comments and suggestions. AP and MB acknowledge the financial support to this research provided by the *Ministero dell’Istruzione, dell’Università e della Ricerca* (MIUR) under the national program *PRIN05 2005024090_002*. NR is supported by an NWO Veni Fellowship, and MAM acknowledges support from WVEPSCoR. This work was supported in part by SAO grant G05-6044.

REFERENCES

- Anders, E., & Grevesse, N. 1989, *Geochim. Cosmochim. Acta*, 53, 197
Arons, J. 1981, *ApJ*, 248, 1099
Arons, J., & Tavani, M. 1993, *ApJ*, 403, 249
Bogdanov, S., Grindlay, J.E., & Rybicki, G.B. 2006, *ApJ*, 648, L55
Burgay, M., et al. 2003, *Nature*, 426, 531
Campana, S., Possenti, A., & Burgay, M. 2004, *ApJ*, 613, L53
Chatterjee, S., Goss, W. M., & Brisken, W.F. 2005, *ApJ*, 634, 101
Chatterjee, S., Gaensler, B.M., Melatos, A. Brisken, W.F., & Stappers, B.W. 2007, *ApJ*, 670, 1301
Cheng, A.F., & Ruderman, M.A. 1980, *ApJ*, 235, 576
Cheng, K.S., & Zhang, L. 1999, *ApJ*, 515, 337
Cheng, K.S., Taam, R.E., & Wang, W. 2006, *ApJ*, 641, 427
Cordes, J.M., & Lazio, T.J.W., 2002, preprint (astro-ph/0207156)
de Jager, O.C., Swanepoel, J. W.H., & Raubenheimer, B.C. 1989, *A&A*, 221, 180
Dickey, J.M., & Lockman, F.J. 1990, *ARA&A*, 28, 215
Gaensler, B.M., & Slane, P.O. 2006, *ARA&A*, 44, 17
Gehrels, N. 1986, *ApJ*, 303, 336
Geppert, U., Küker, M., Page, D. 2006, *A&A*, 457, 937
Gonzalez, M. E., Kaspi, V. M., Camilo, F., Gaensler, B. M., Pivovarov, M. J. 2005, *ApJ*, 630, 489
Granot, J., & Mészáros, P. 2004, *ApJ*, 609, L17
Grindlay, J.E., Camilo, F., Heinke, C.O., Edmonds, P.D., Cohn, H., & Lugger, P. 2002, *ApJ*, 581, 470
Harding, A.K., Ussov, V.V., & Muslimov, A.G. 2005, *ApJ*, 622, 531
Harding, A.K., & Muslimov, A.G. 2002, *ApJ*, 568, 862
Kaplan, D.L., van Kerkwijk, M.H., & Anderson, J. 2007, *ApJ*, 660, 1428
Kargaltsev, O., Pavlov, G.G., & Garmire G.P. 2006, *ApJ*, 646, 1139
Kennel, C.F., & Coroniti, F.V. 1984, *ApJ*, 283, 694
Kramer, M., et al. 2006, *Science*, 314, 97
Li, X-H., Lu, F-J. & Li, Z. 2007, *ApJ*, submitted (arXiv:0707.4279)
Lodders, K. 2003, *ApJ*, 591, 1220

²⁰ As an alternate option, Kargaltsev et al. (2006) suggest that the orbital X-ray modulation seen in PSR B1534+12 is due to the misalignment between the equatorial plane of the recycled pulsar and the binary orbit. This misalignment may be larger for the B1534+12 system than for the J0737–3039 system.

- Lorimer, D. R., et al. 2007, MNRAS, 379, 1217
 Lyne, A. G., et al. 2004, Science, 303, 1153
 Lyutikov, M. 2004, MNRAS, 353, 1095
 McLaughlin, M. A., et al. 2004a, ApJ, 613, L57
 McLaughlin, M. A., et al. 2004b, ApJ, 616, L131
 McLaughlin, M. A., et al. 2004c, ApJ, 605, L41
 McClure-Griffiths, N. M., Dickey, J. M., Gaensler, B. M., & Green, A. J. 2004, ApJ, 607, 127
 Page, D., & Sarmiento, A. 1996, ApJ, 473, 1067
 Pellizzoni, A., De Luca, A., Mereghetti, S., Tiengo, A., Mattana, F., Caraveo, P., Tavani, M., & Bignami, G.F. 2004, ApJ, 612, L49
 Pellizzoni, A., Tiengo, A., De Luca, A., Esposito, P., & Mereghetti, S. 2008, ApJ, in press, (arXiv:0802.0350)
 Possenti, A., Cerutti, R., Colpi, M., & Mereghetti, S. 2002, A&A, 387, 993
 Psaltis, D., zel, F., & DeDeo, S. 2002, ApJ, 544, 390
 Saito, Y., Kawai, N., Kamae, T., Shibata, S., Dotani, T., & Kulkarni, S.R. 1997, ApJ, 447, L37
 Stairs, I.H., Thorsett, S.E., Taylor, J.H., & Wolszczan, A. 2002, ApJ, 581, 501
 Turolla, R., & Treves, A. 2004, A&A, 426, L1
 Yakovlev, D. G., & Pethick, C. J., 2004, Ann. Rev. A&A, 42, Issue 1, 169
 Zhang, B., & Harding, A.K. 2000, ApJ, 532, 1150
 Zavlin, V.E., Pavlov G.G, & Shibanov, Yu.A. 1996, A&A, 315, 141
 Zavlin, V.E., & Pavlov, G.G, 1998, A&A, 329, 583
 Zavlin, V.E. 2006, ApJ, 638, 951

TABLE 1
OBSERVATIONS OF THE PSR J0737–3039 SYSTEM

Instrument	Start date	Tot exp ^a (ks)	Tot Source (Bkg) ^b (counts)	Orbits ^c	Source (Bkg) ^d (counts)	Analysis ^e	Ref ^f
Chandra ACIS-S	2004/01/18	10.0	70 (1)	1	64 (1)	t,p	(1),(4)
XMM MOS1+MOS2 ^g	2004/04/10	47.2	549 (155)	5+4	432 (110)	t,s	(2),(3),(4)
Chandra HRC-S	2006/02/28	53.5	251 (5)	6	250 (5)	t,p	(5)
Chandra HRC-S	2006/03/02	35.8	169 (6)	4	167 (6)	t,p	(5)
Chandra ACIS-S	2006/06/06	79.0	534 (3)	9	529 (3)	t,p,s	this work

Note. — Observations used for spectral, spatial and timing analysis.

^a Total exposure times calculated after cleaning for spurious flares (for *XMM-Newton*), but not including dead-time corrections.

^b The source (and background: Bkg) counts are reported in the bands used for the timing analysis: 0.3–8 keV (*Chandra*) and 0.3–2.2 keV (*XMM-Newton*). The background dominates above 2.2 keV in the *XMM-Newton* band (Pellizzoni et al. 2004). The time resolutions are 16 μ s for HRC-S, 2.6 s for MOS1+MOS2, and 3.241 s for ACIS-S.

^c Number of sampled full orbits.

^d The source (and background: Bkg) counts refer to the number of completely sampled orbits of column 5.

^e Analysis which a dataset has been used for in this work: p=spectral; s=spectral; t=timing.

^f References: (1) McLaughlin et al. 2004c; (2) Campana et al. 2004; (3) Pellizzoni et al. 2004; (4) Kargaltsev et al. 2006; (5) Chatterjee et al. 2007.

^g The photons collected with the PN detector (operated in timing mode) have not been included in our analysis, since they are largely background dominated (Pellizzoni et al. 2004).

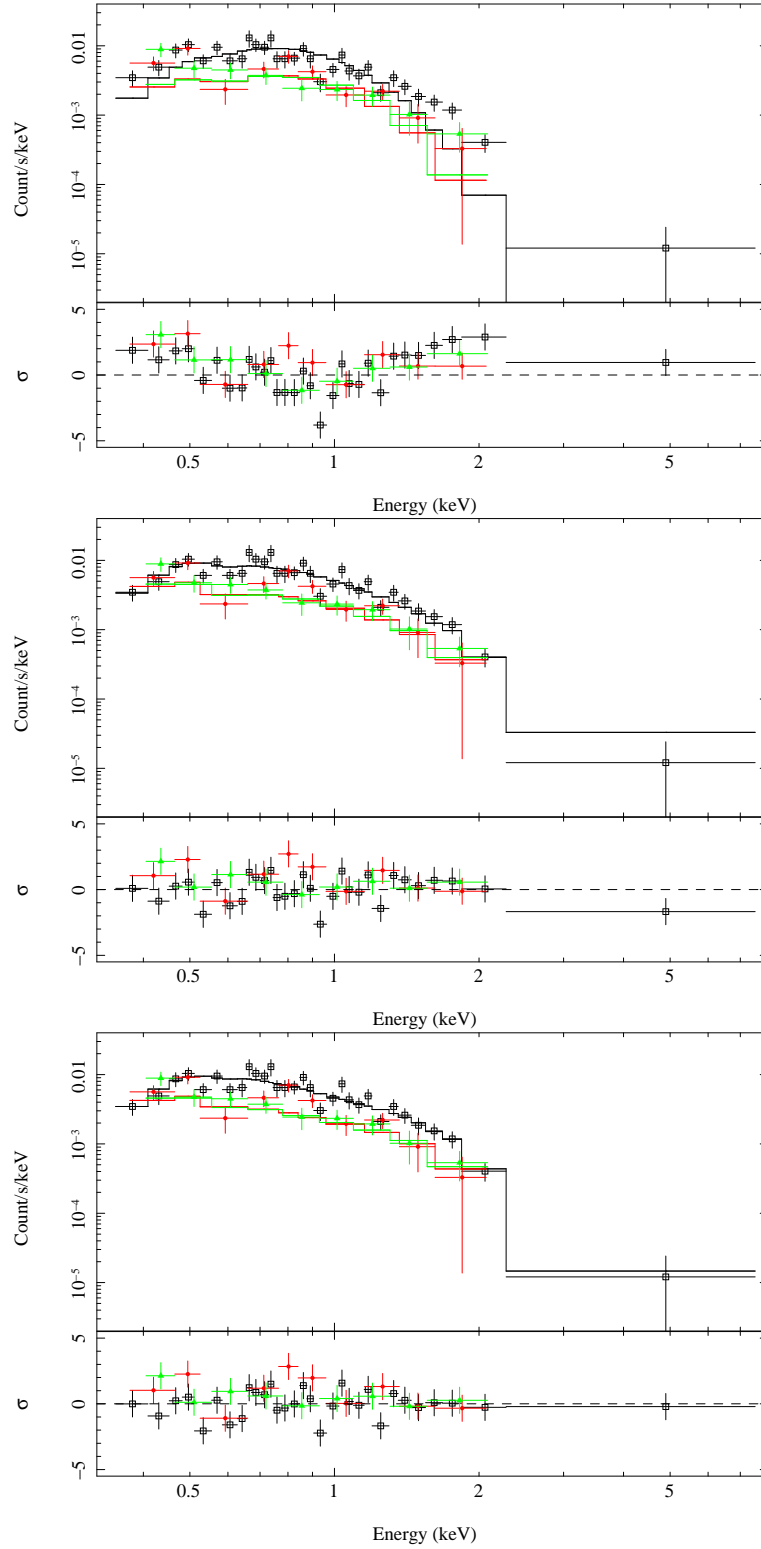


FIG. 1.— Spectra (top panels) and residuals (bottom panels) of the spectral modeling of the J0737–3039 system obtained from the 2006 June *Chandra* ACIS-S (black squares) and the 2004 April *XMM–Newton* MOS1 (red filled circles) and MOS2 (green filled triangles) observations. The data have been modeled with an absorbed blackbody (top figure), power-law (middle figure) and two blackbodies (bottom figure; see Table 2 for details). Solid lines are the fitted models.

TABLE 2
SPECTRAL PARAMETERS FOR THE PSR J0737–3039 SYSTEM

Model	BB	PL	Bremss	BB+PL	BB+BB	Comptonized BB
N_H^a	< 0.1	1.6 ± 0.6	< 0.1	1.5 ± 0.8	< 0.1	< 0.1
$\Gamma/kT_1/kT_2^b$	0.18 ± 0.05	3.7 ± 0.4	0.6 ± 0.1	$3.7 \pm 0.5/0.18^e$	$0.10 \pm 0.01/0.30 \pm 0.05$	0.07 ± 0.03^f
Flux ^c	2.5 ± 1	8 ± 1	3 ± 1	8 ± 1	5 ± 1	5 ± 1
Luminosity ^d	0.7 ± 0.3	2.4 ± 0.3	0.9 ± 0.3	2.4 ± 0.3	1.5 ± 0.3	1.5 ± 0.3
χ^2_ν ; d.o.f.; n.h.p.	2.32; 47; 10^{-7}	1.25; 47; 0.09	1.27; 47; 0.08	1.29; 46; 0.07	1.23; 45; 0.08	1.25; 45; 0.18

Note. — Parameter values of the spectral models discussed in the text. Errors are reported at 90% confidence level.

^a N_H is in units of 10^{21} cm^{-2} assuming solar abundances from Lodders (2003).

^b kT_1 and kT_2 are in keV.

^c Fluxes are unabsorbed, calculated in the 0.3–8 keV energy range, and reported in units of $10^{-14} \text{ ergs s}^{-1} \text{ cm}^{-2}$.

^d Luminosities are expressed in units of $10^{30} \text{ ergs s}^{-1}$ and are calculated for isotropic emission at a distance of 500 pc.

^e This temperature corresponds to the smallest χ^2 value in a pure blackbody fit, even though the fit is not acceptable. Here it was held fixed at this value.

^f The value of the optical depth for the best fit is $\tau = 1.5 \pm 0.6$ for a thermal electron bath with energy $kT_e = 10 \pm 5 \text{ keV}$

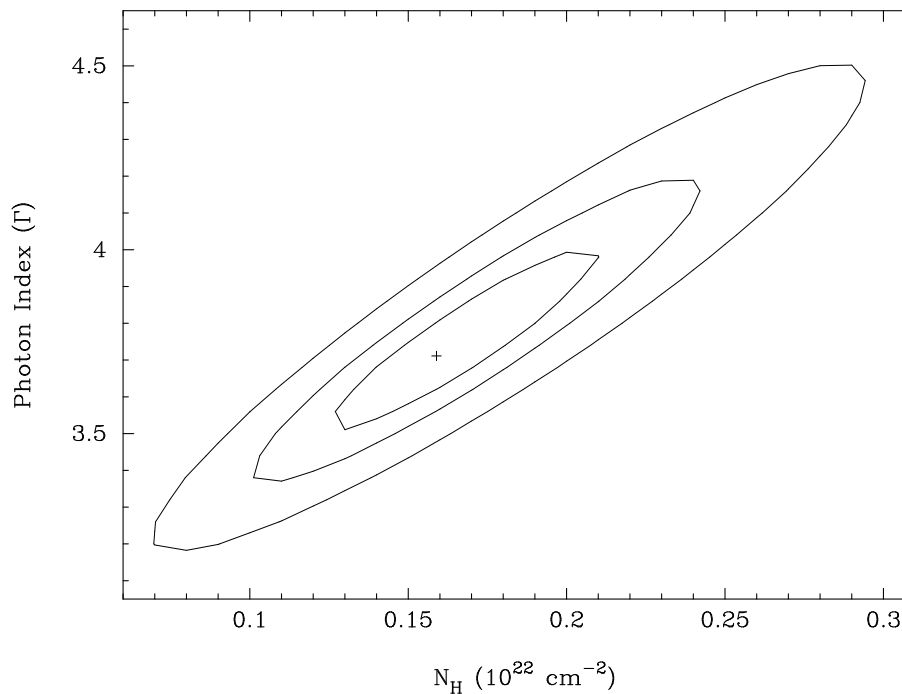


FIG. 2.— Contour plot of N_H vs Γ for the absorbed power-law spectral model (see Table 2). The cross represents the best fit values, and the ellipses report (from smallest to largest) the 68%, 90% and 99% confidence level contours on the parameters.

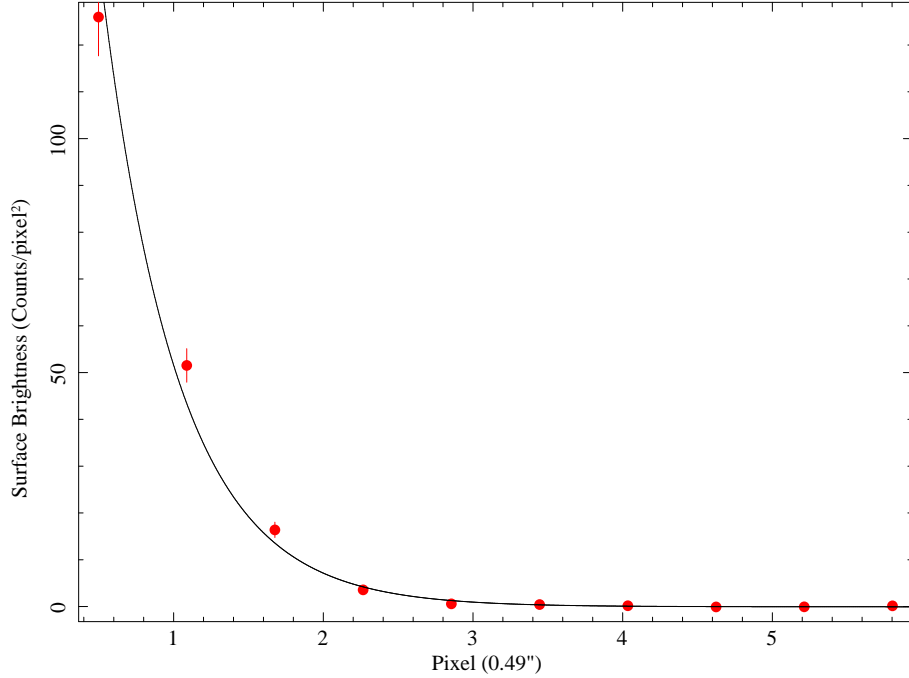


FIG. 3.— *Chandra* ACIS-S one dimensional profile of the J0737-3039 system (filled circles) superimposed with the simulated instrumental PSF (solid line).

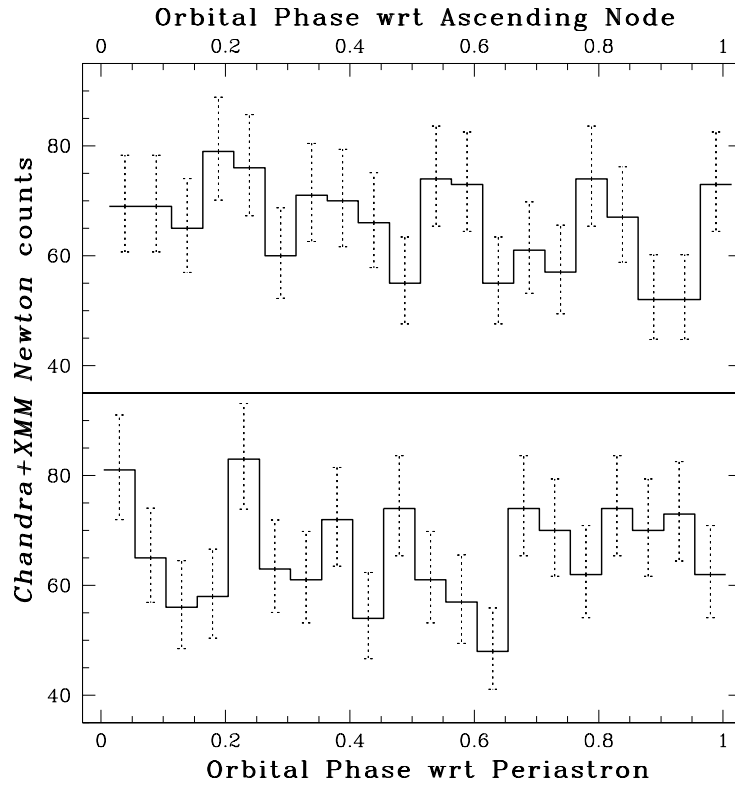


FIG. 4.— Background-subtracted X-ray orbital light-curves for the J0737-3039 system. The histograms are obtained by folding into 20 bins all the photons collected so far by *Chandra* and *XMM-Newton* (see Table 1). The error-bars are plotted following the prescription of Gehrels (1986). In the lower panel, phase=0.0 is set at the periastron of PSR J0737-3039A and the center of the first bin is at phase=0.030, while in the upper panel phase=0.0 corresponds to the ascending node of the orbit of PSR J0737-3039A and the center of the first bin is at phase=0.039.